

# Effects of pulling speed and hot zone temperature on the directional growth of $\text{YBa}_2\text{Cu}_3\text{O}_x$ superconductor

KWANGSOO NO, WOO SUCK SHIN

*Department of Ceramic Science and Engineering, Korea Advanced Institute of Science and Technology, Daejeon, Korea*

WONBAEK KIM, GUNCHOO SHIM

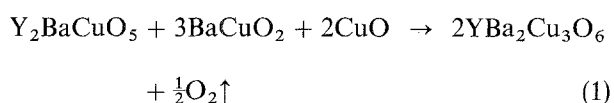
*Korea Institute of Geology, Mining and Materials, Daejeon, Korea*

The effects of pulling speed and hot zone temperature on the microstructure and the superconducting properties of  $\text{YBa}_2\text{Cu}_3\text{O}_x$  sample textured using directional growth of  $\text{Y}_2\text{BaCuO}_5$ ,  $\text{BaCuO}_2$ , and  $\text{CuO}$  powder mixture were studied. The grain size, the alignment, and the critical current density of the sample were increased as the pulling speed decreased. The sample grown directionally at  $1.5 \text{ mm h}^{-1}$  pulling speed consisted of a single grain. The zero resistivity temperature and the critical current density of the sample increased as the hot zone temperature increased up to  $1120^\circ\text{C}$  beyond which the sample consisted of  $\text{Y}_2\text{O}_3$  and impurities and showed resistivity at 77 K. The sample grown directionally at  $1.5 \text{ mm h}^{-1}$  pulling speed and at  $1120^\circ\text{C}$  hot zone temperature showed sharp resistivity transition of 91 K zero resistivity and over  $6000 \text{ A cm}^{-2}$ . The sample showed well aligned microstructure. Compared to data from another study, the hot zone temperature required to produce maximum critical current density is lower due to low liquid forming temperature.

## 1. Introduction

Progress toward major applications of the bulk high temperature superconductor has been hindered by low transport critical current densities ( $J_C$ ) at the boiling point of liquid nitrogen and their severe degradation in weak magnetic fields because of the weak link problem in the sintered materials [1]. Several studies [2–4] have succeeded in reducing the weak link problem in bulk samples employing a melt and directional solidification process which enables the fabrication of well-textured samples with clean boundaries and large grains aligned in a preferred orientation. Those samples exhibited dramatically improved transport  $J_C$  values at the boiling point of liquid nitrogen of above  $10^4 \text{ A cm}^{-2}$  in zero magnetic field ( $H$ ) and of above  $10^3 \text{ A cm}^{-2}$ ,  $H = 1 \text{ T}$  as compared to several hundred and about  $1 \text{ A cm}^{-2}$ , respectively, for the samples without the texturing.

A technique has been found for preparing 123 ceramics by reacting  $\text{Y}_2\text{BaCuO}$  (211),  $\text{BaCuO}_2$  (011), and  $\text{CuO}$  (001) precursor powder mixture with the following reaction [5]



This reaction involves two melt forms, one beginning at  $\sim 950^\circ\text{C}$  and one at  $\sim 980^\circ\text{C}$ , representing

$011 + 001 \rightarrow \text{liquid}$  and  $211 + 011 \rightarrow 202 + \text{liquid}$ , respectively. Those melt forms provide a faster reaction than the reaction involving only interatomic diffusion in the solid state sintering technique. Above  $\sim 1015^\circ\text{C}$ , 123 was found to melt incongruently forming liquid and 211 [6].

In a former paper [7], we reported the texturing of bulk 123 ceramics by directional growth of 123 grains reacted from 211, 011 and 001 precursor powder mixture. The samples consisted of several mm-long grains aligned parallel to the growth direction. The microstructure observation and X-ray diffraction analysis showed that the grains have a preferred orientation to improve the critical current density.

The condition for a stable plane front solidification is [8]

$$\frac{G_i}{R} > \frac{\Delta T}{D_L} \quad (2)$$

where  $G_i$  = temperature gradient in solid-liquid interface,  $R$  = solidification velocity,  $\Delta T = T_1 - T_s$ ,  $T_1$  = liquidus temperature,  $T_s$  = solidus temperature, and  $D_L$  = diffusivity in liquid. Among these parameters, the temperature gradient and the solidification velocity can be easily changed in the directional growth process. The former can be changed by setting different hot zone temperatures, and the latter can be changed by setting different pulling speeds. In this

paper, we report the microstructure and the superconducting properties of bulk  $\text{YBa}_2\text{Cu}_3\text{O}_x$  ceramics textured by directional growth of  $\text{YBa}_2\text{Cu}_3\text{O}_x$  grains reacted from  $\text{Y}_2\text{BaCuO}_5$ ,  $\text{BaCu}$  and  $\text{CuO}$  powder mixture at different pulling speeds and hot zone temperatures.

## 2. Experimental procedure

$\text{Y}_2\text{BaCuO}_5$  and  $\text{BaCuO}_2$  precursor powders were synthesized using solid state reactions of reagent grade  $\text{Y}_2\text{O}_3$ ,  $\text{BaCO}_3$ , and  $\text{CuO}$  powder mixtures. The process conditions for the precursor powders were described in detail in [5]. The mixture of 2:1:1, 0:1:1, and 0:0:1 precursor powders was ground in an automatic agate mortar and pestle for 1 h for each 10 g, and bar samples of the powder mixture with a few drops of organic binder (approximately  $0.3 \times 0.1 \times 3$  cm in dimensions) were pressed in a steel mould. After drying in air overnight, the bar samples were carefully heat treated at  $850^\circ\text{C}$  for 1 h to calcine the organic binder and to provide enough strength for handling. A small hole was drilled at one side of the heat-treated bar sample in order to hang the sample on a constant speed puller using platinum wire. The bar samples were pulled up at different speeds through a high temperature zone of which temperature was maintained using a small platinum coil inside a kanthal furnace as shown in Fig. 1. The hot zone temperature was varied using the platinum coil current while the temperature of the kanthal furnace was kept at constant value. Fig. 1 also shows a temperature profile at  $1070^\circ\text{C}$  hot zone temperature. The temperature profile was measured with a standard thermocouple. The standard thermocouple attached to the puller was kept at each point for 10 min to read static temperatures.

After cooling down to room temperature, both flat surfaces of the bar sample were ground using SiC paper, and the sample was cut in half using a diamond saw, one half for superconducting property measurements and the other for microstructural examinations. Four electrical contacts on the superconducting property measurement sample were made of silver epoxy, and then both samples were heat treated to provide better contact between the superconductor and silver epoxy in an oxygen flowing atmosphere at  $800^\circ\text{C}$  for

1 h. During cooling to room temperature, the sample was held at  $550^\circ\text{C}$  for 24 h in order to provide 123 with appropriate oxygen stoichiometry.

The superconductivity transition temperatures and the critical current densities of the samples were measured using d.c. four-point probe method. The lead wires carrying the current were attached to the silver contacts using soldering for the critical current density measurements in liquid nitrogen. The voltage drop across inner two electrical contacts was measured using a Keithley 181 nanovoltmeter, and the temperatures were measured using a diode temperature sensor.

The crystallographic orientation of the textured samples were identified using X-ray diffraction analyses and microstructure observations.

## 3. Results and discussion

According to Equation 2, the plane front solidification is stable at low solidification velocity and high temperature gradient. The solidification velocity can be controlled by setting different pulling speeds. Fig. 2 shows polarized light images of the samples grown directionally at the same hot zone temperature ( $1120^\circ\text{C}$ ) but at different pulling speeds. Large grain structure in the sample is observed on different contrast in the polarized light. The grain size increased as the pulling speed decreased (as the solidification velocity decreased). The sample grown at  $1.5 \text{ mm h}^{-1}$  pulling speed (Fig. 2(c)) consists of two grains. Because portions of the samples grown in the later part of the process consisted of larger grains and better alignment, these portions (approximately 1 cm in length) were used to measure the critical temperature and the critical current density. Fig. 3 shows current density versus voltage curves of a sample (sintered at  $980^\circ\text{C}$ ) showing a typical grain size and random microstructure and the samples grown directionally at the same hot zone temperature ( $1120^\circ\text{C}$ ) but at different pulling rates. The sintered sample showed the critical current density of about  $60 \text{ A cm}^{-2}$ . Compared with the value of the sintered sample, the directionally grown samples showed improved critical current density. As the pulling rate decreased, the critical current density increased. The sample grown at  $1.5 \text{ mm h}^{-1}$  showed the critical current density of over  $1800 \text{ A cm}^{-2}$  which is the maximum current applying capability of the instrument used in this study. As pulling speed decreased, the plane front solidification became stable, the number of grain boundaries which served as weak links decreased, and the sample carried higher current.

The plane front solidification is stable at high temperature gradient which can be achieved at high hot zone temperatures. So it was expected that the alignment of the grain and superconducting properties would be improved as the hot zone temperature increased. Fig. 4 shows temperature versus resistivity curves of a sintered sample and the samples grown directionally at the same pulling rate ( $1.5 \text{ mm h}^{-1}$ ) but at different hot zone temperatures. The sintered sample and the sample grown at  $950^\circ\text{C}$  hot zone temperature showed tails in the transition region and

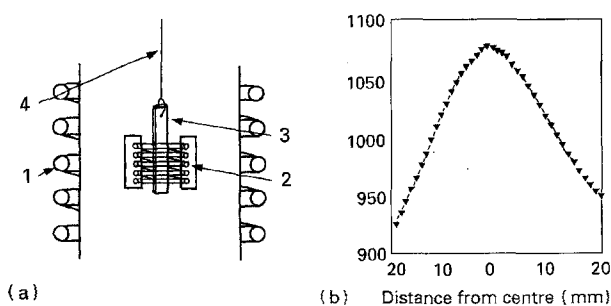


Figure 1 (a) A schematic diagram of directional growth furnace, where 1 is a kanthal furnace, 2 is a platinum coil furnace, 3 is a sample, and 4 is platinum wire, and (b) a temperature profile at  $1070^\circ\text{C}$  hot zone temperature.

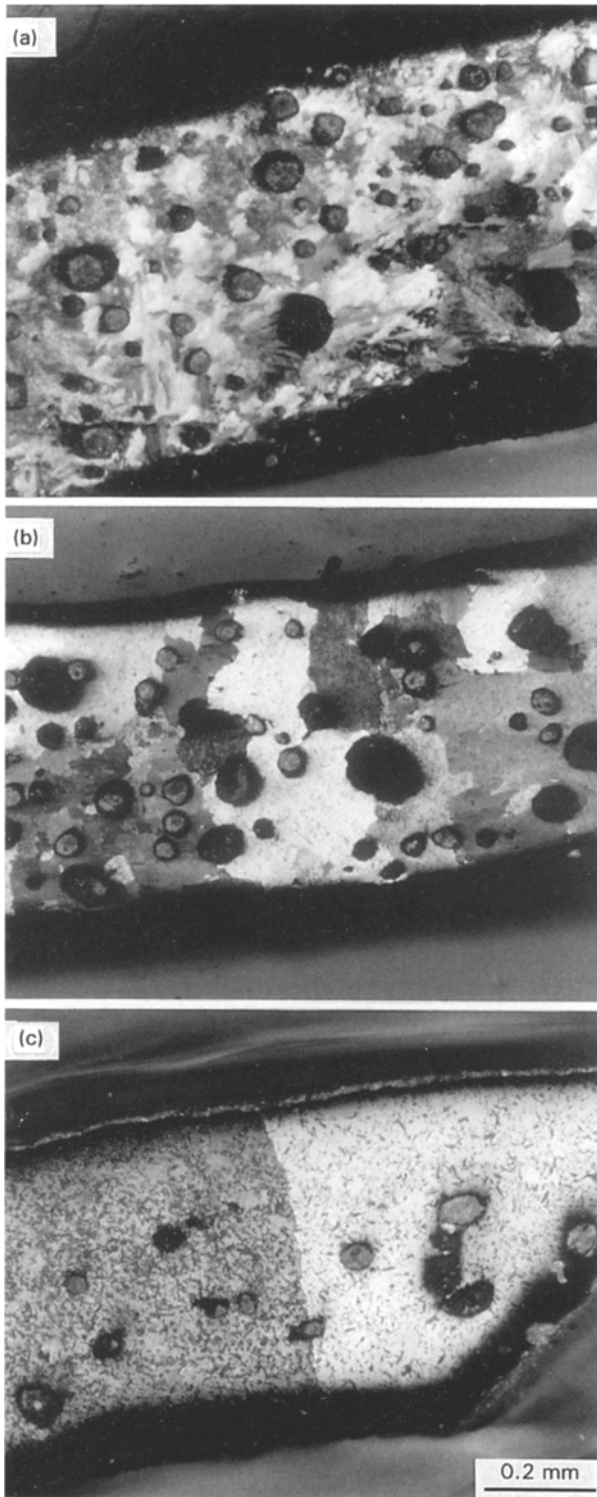


Figure 2 Polarized light images of  $\text{YBa}_2\text{Cu}_3\text{O}_x$  samples grown directionally at  $1120^\circ\text{C}$  hot zone temperature but at different pulling speeds: (a)  $10\text{ mm h}^{-1}$ , (b)  $6.3\text{ mm h}^{-1}$ , and (c)  $1.5\text{ mm h}^{-1}$ . The surfaces are perpendicular to the growth direction. The white bar represents  $0.2\text{ mm}$ .

zero resistivity at around  $88\text{ K}$ . As the hot zone temperature increased, the zero resistivity temperature increased. This observation corresponds to the observation made in [5] and may be due to the fact that the reactivity of the reaction in Equation 1 increased at high temperature. The sample grown at  $1120^\circ\text{C}$  hot zone temperature showed very sharp resistivity transition and zero resistivity at  $91\text{ K}$ . But the sample grown at  $1155^\circ\text{C}$  hot zone temperature showed resis-

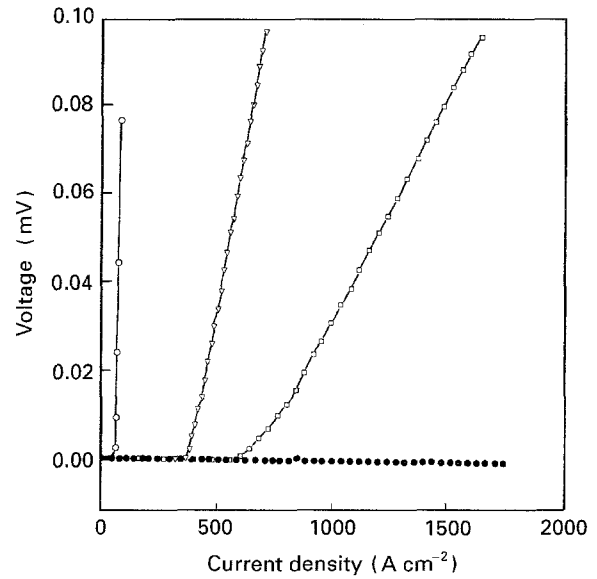


Figure 3 Current density versus voltage curves of a sample sintered at  $980^\circ\text{C}$  and the samples grown directionally at  $1120^\circ\text{C}$  hot zone temperature but at different pulling speeds.  $\circ$  sintered;  $\nabla$   $10\text{ mm h}^{-1}$ ;  $\square$   $6.3\text{ mm h}^{-1}$ ;  $\bullet$   $1.5\text{ mm h}^{-1}$ .

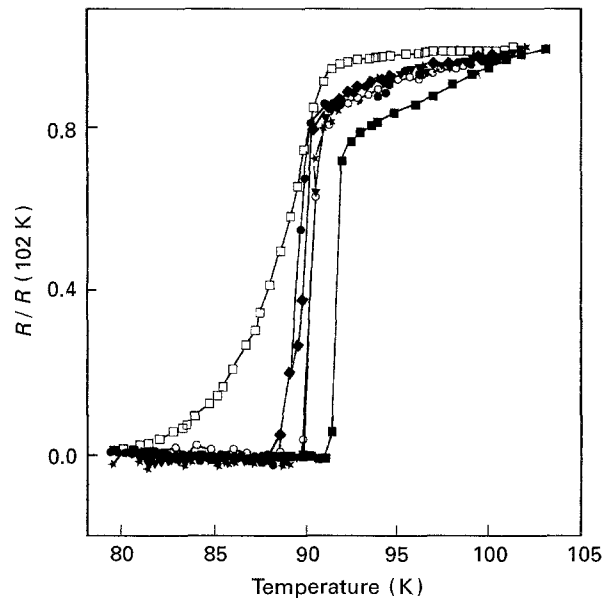


Figure 4 Temperature versus resistivity curves of a sintered sample and the samples grown directionally at the same pulling speed ( $1.5\text{ mm h}^{-1}$ ) but at different hot zone temperatures.  $\blacklozenge$  sintered;  $\bullet$   $950^\circ\text{C}$ ;  $\circ$   $1010^\circ\text{C}$ ;  $\blacktriangledown$   $1075^\circ\text{C}$ ;  $\star$   $1085^\circ\text{C}$ ;  $\blacksquare$   $1120^\circ\text{C}$ ;  $\square$   $1155^\circ\text{C}$ .

tivity even at  $77\text{ K}$ . Fig. 5 shows the microstructure of the sample grown at  $1155^\circ\text{C}$ . The sample consisted of mainly impurities and voids. X-ray diffraction analysis showed that the sample consisted of  $\text{Y}_2\text{O}_3$  and unidentified impurities. Microstructure observation and X-ray diffraction analysis indicates that the hot zone temperature of  $1155^\circ\text{C}$  was high enough to decompose the sample into  $\text{Y}_2\text{O}_3$  and liquid.  $\text{YBa}_2\text{Cu}_3\text{O}_x$  was reported to melt incongruently forming liquid and  $\text{Y}_2\text{O}_3$  at  $1270^\circ\text{C}$ . The incongruent melting temperature observed in this study was over  $100^\circ\text{C}$  lower than the reported value.

Fig. 6 shows hot zone temperature versus critical current density curves of the samples grown directionally at different hot zone temperatures. As the hot

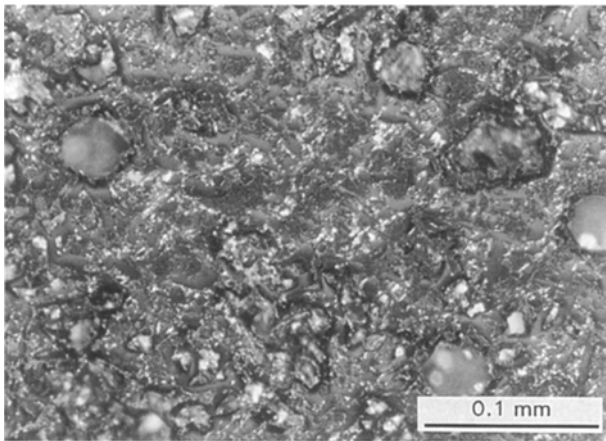


Figure 5 A polarized light image of the sample grown at 1155 °C. The white bar represents 0.1 mm.

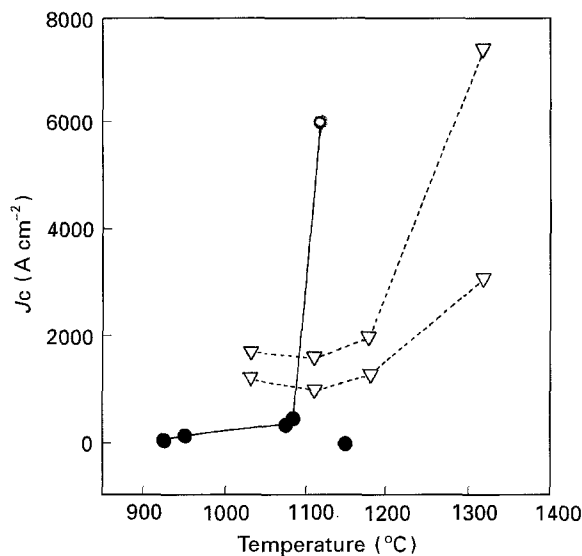


Figure 6 Hot zone temperature versus critical current density curves of the samples grown at different hot zone temperatures. The open circle indicates that the value was lower than the real  $J_c$  which could not be measured due to the limitation of the current supply used in this study. ● This study; ▽ Jin *et al.* [9].

zone temperature increased, the critical current density increased. This observation may be due to two effects. As hot zone temperature increased, the reactivity of the reaction in Equation 1 increased, and the sample consisted of less impurities impeding the current flow. And as hot zone temperature increased, the plane front solidification became stable, and the number of grain boundaries which served as weak links decreased. The sample grown at 1120 °C hot zone temperature showed a critical current density of over 6000 A cm<sup>-2</sup> which is the maximum current applying capability of the instrument used in this study. The sample grown at 1155 °C showed resistivity at 77 K and zero critical current density at the boiling point of liquid nitrogen. In order to compare with this study, the data from Jin *et al.* [9] were also included in the figure. Both curves show critical current jumps at certain hot zone temperatures. The hot zone temperature at which a maximum critical current density showed occurred at about 200 °C lower in this study than in the data from Jin *et al.* A significant difference

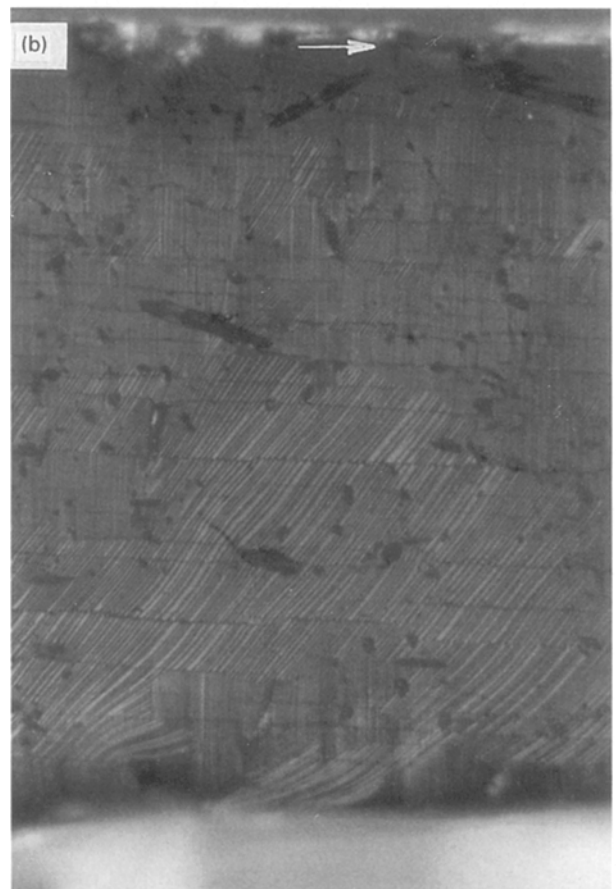
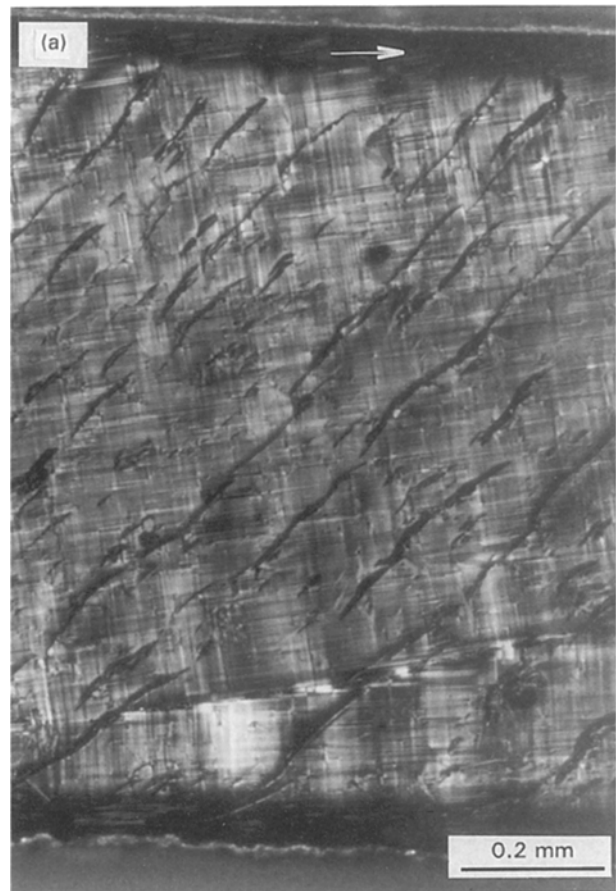


Figure 7 Polarized light images of the sample grown directionally at 1120 °C hot zone temperature. (a) One side of the sample and (b) the other side of the sample. The growth direction is indicated in the figure. Arrows indicate the growth direction, and the white bar represents 0.2 mm.

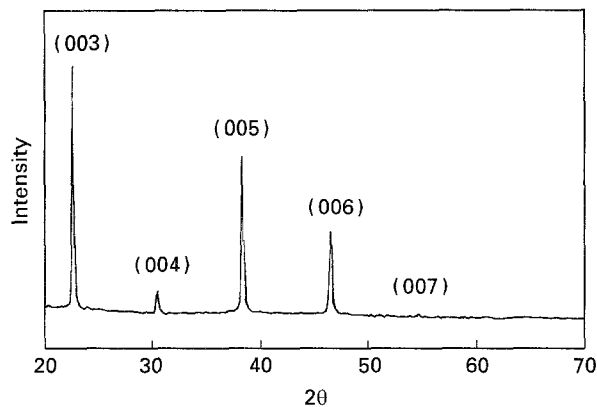


Figure 8 The X-ray diffraction pattern of the surface shown in Fig. 7(a).

between Jin *et al.*'s work and this study was the precursor power used. Jin *et al.* used reacted  $\text{YBa}_2\text{Cu}_3\text{O}_x$  power, but this study used  $\text{Y}_2\text{BaCuO}$ ,  $\text{BaCuO}_2$  and  $\text{CuO}$  powder mixture. The powder mixture used in this study form liquid at lower temperatures, and the liquid may decrease the hot zone temperature for a maximum critical current density.

Fig. 7 shows the microstructure of the sample grown directionally at  $1120^\circ\text{C}$  hot zone temperature. The sample showed well-aligned grain structure. One side of the sample (Fig. 7(a)) consists of cross-check twins, and the other side (perpendicular to the former, Fig. 7(b)) consists of line twins. These observations indicate that the one side of the sample (Fig. 7(a)) is parallel to the basal plane and that the other side of the sample (Fig. 7(b)) is perpendicular to the basal plane. This sample alignment is ideal for high current flowing capability because the current is applied through the growth direction which is parallel to the  $a$ - $b$  basal plane. Two kinds of cracks were observed in the microstructures. One kind slants to the growth direction on one side of the sample (Fig. 7(a)), and the other is parallel to the growth direction on the other side of the sample (Fig. 7(b)). The slant cracks appear to be induced during the polishing of the sample because they are not observed on the other side of the sample. Because the current flow parallel to the growth direction, the parallel crack may not significantly affect the critical current density.

The orientation of one surface of the sample (Fig. 7(a)) was examined using X-ray diffraction. Fig. 8 shows the X-ray diffraction pattern from the surface. Only (00 $l$ ) peaks were observed in the pattern without any detectable impurity, indicating the surface mainly consists of the basal plane of pure  $\text{YBa}_2\text{Cu}_3\text{O}_7$ , which corresponds to the observations made in the microstructural examination. The relative

intensities of the peaks were not matched to the reported standard X-ray diffraction pattern, but the intensity of (003) peak is higher than the other peaks. This observation was not explained in this study, and further study is required.

#### 4. Summary

Studying the effects of pulling speed and hot zone temperature on the microstructure and the superconducting properties of  $\text{YBa}_2\text{Cu}_3\text{O}_x$  sample texture using directional growth of  $\text{Y}_2\text{BaCuO}_5$ ,  $\text{BaCuO}_2$  and  $\text{CuO}$  powder mixture, we reach the following conclusions.

1. The grain size, the alignment and the critical current density of the sample were increased as the pulling speed decreased. The sample grown directionally at  $1.5 \text{ mm h}^{-1}$  pulling speed consisted of a single grain.

2. The zero resistivity temperature and critical current density of the sample increased as the hot zone temperature increased up to  $1120^\circ\text{C}$  beyond which the sample consisted of  $\text{Y}_2\text{O}_3$  and impurities and showed resistivity even at 77 K. The sample grown directionally at  $1.5 \text{ mm h}^{-1}$  pulling speed and at  $1120^\circ\text{C}$  hot zone temperature showed a sharp resistivity transition of 91 K zero resistivity and over  $6000 \text{ A cm}^{-2}$ . The sample showed well-aligned microstructure.

3. Compared to the data of other studies, the hot zone temperature required to produce maximum critical current density is lower due to low liquid forming temperature.

#### References

1. J. W. EKIN, *Adv. Ceram. Mater.* **2** (1987) 586.
2. S. JIN, H. TIEFEL, R. C. SHERWOOD, M. E. DAVIS, R. B. VAN DOVER, G. W. KAMMLOTT, R. A. FASTNACHT and H. D. KEITH, *Appl. Phys. Lett.* **52** (1988) 2074.
3. P. J. MCGINN, M. A. BLACK and A. VALENZUELA, *Phys. C* **156** (1988) 57.
4. M. MURAKAMI, M. MORITA, K. DOT and K. MIYAMOTO, *Jpn J. Appl. Phys.* **28** (1989) 1189.
5. K. NO, D. S. CHUNG, J. M. KIM, H. Y. KIM and G. SHIN, *J. Mater. Sci.* **26** (1991) 3593.
6. T. ASELAGÉ and K. KEEFER, *J. Mater. Res.* **3** (1988) 1279.
7. K. NO, D. S. CHUNG and J. M. KIM, *ibid.* **5** (1990) 2610.
8. Z. JISHAN *et al.*, *Supercond. Sci. Tech.* **1** (1988) 107.
9. S. JIN *et al.*, *Phys. Rev. B* **37** (1988) 7850.

Received 12 April  
and accepted 21 September 1994